Catalysis Today 164 (2011) 262–267

Contents lists available at ScienceDirect

Catalysis Today

journal homepage: www.elsevier.com/locate/cattod

Oxidative steam reforming of ethanol over carbon nanofiber supported Co catalysts

Andre L.M. da Silva[a], Lisiane V. Mattos[a,1], Johan P. den Breejen[b], Johannes H. Bitter[b], Krijn P. de Jong[b], Fábio B. Noronha[a,*]

[a] Instituto Nacional de Tecnologia – INT, Av. Venezuela 82, CEP, 20081-312 Rio de Janeiro, Brazil
[b] Inorganic Chemistry and Catalysis, Debye Institute of Nanomaterials Science, Utrecht University, Sorbonnelaan 16, 3508 Utrecht, The Netherlands

ARTICLE INFO

Article history:
Received 2 July 2010
Received in revised form 30 October 2010
Accepted 2 November 2010
Available online 8 December 2010

Keywords:
Fuel cell
Hydrogen production
Oxidative steam reforming of ethanol
Co/CNF
Particle size effect

ABSTRACT

The effect of the cobalt particle size in the ethanol oxidative steam reforming reaction for hydrogen production was investigated using cobalt on carbon nanofiber catalysts. The smallest (<4 nm) particles showed a significantly larger amount of acetaldehyde and smaller amount of H_2 as compared to larger ones. This result indicated that the C–C cleavage is more difficult on small Co particles under OSR conditions, which was due to a higher extent of surface oxidation of smaller particles in this reaction. The catalysts with larger Co particles (>4 nm) were quite stable during OSR reaction but significant carbon formation was detected.

1. Introduction

Co-based catalysts have been extensively studied for the steam reforming (SR) of ethanol [1–11], since cobalt is a low-cost alternative to noble metals. In spite of the high activity of Co-based catalysts, there is scarce information about the effect of cobalt particle size on the catalyst activity and stability for the SR reaction. In fact, only few works report the data of surface-specific activity, the so-called turnover frequency (TOF), as a function of metal dispersion [10,11].

The main reason for this lack of knowledge is likely due to difficulties in distinguishing between apparent and real particle size effects. One significant complication is that most of the metal oxides used as catalyst support are active for the SR reaction. In spite of their lower activity relative to supported metal catalysts, a wide range of undesirable by-products (e.g., ethylene, acetaldehyde and acetone) is formed during SR of ethanol over metal oxides in comparison with supported metal catalysts, depending on the metal oxide properties. For example, Al_2O_3 is generally used as a support but its acid sites promote dehydration of ethanol to ethylene [12]. MgO contains basic sites, which are proposed to be highly selective for ethanol dehydrogenation to acetaldehyde [3]. The partially reducible oxides CeO_2 [13] and $CeZrO_2$ [14] are highly active for the SR, producing very low CO concentration. In addition, depending on the support, cobalt oxide reduction may be hindered due to strong interactions between cobalt oxides (especially CoO) with the support or through the formation of irreducible mixed oxides such as cobalt aluminate during the calcination or activation steps. The presence of these phases may result in the loss of activity since metallic cobalt is considered to be the active site for the SR reaction [15]. Actually, alumina supported catalysts containing low cobalt loading favor the formation of small Co particles, which are more difficult to reduce due to the stronger interaction with the support [16]. Therefore, the lower activities of the catalysts containing small particles may not be directly attributed to a particle size effect.

The careful elimination of these artifacts is fundamental in order to understand the intrinsic cobalt particle size effects on SR of ethanol activity and selectivity. Therefore, the study of cobalt particle size effects has to be undertaken using an inert support such as carbon based materials. However, only few studies investigated the performance of carbon supported catalysts [17–19] and multiwall carbon nanotubes [20] for SR of ethanol. Galvita et al. [17,18] reported that Pd/C is an active catalyst for ethanol decomposition to CH_4, H_2 and CO. Haga et al. [19] also concluded that ethanol decomposition is the main reaction taking place during SR of ethanol at 673 K over Co/C catalyst. Barthos et al. [20] studied the SR of

* Corresponding author. Tel.: +55 21 2123 1177; fax: +55 21 2123 1166.
E-mail addresses: k.p.dejong@uu.nl (K.P. de Jong), fabio.bellot@int.gov.br, fabiobel@int.gov.br (F.B. Noronha).
[1] Present address: Universidade Federal Fluminense (UFF) – Departamento de Engenharia Química e de Petróleo Rua Passo da Pátria, 156-CEP 24210-240 Niterói, RJ, Brasil.

0920-5861/$ – see front matter © 2010 Elsevier B.V. All rights reserved.
doi:10.1016/j.cattod.2010.11.013

ethanol at 723 K over Mo_2C supported on carbon nanotubes (CNTs). In this case, hydrogen and acetaldehyde were the main products formed due to the ethanol dehydrogenation reaction. In addition, the catalyst strongly deactivated during SR, with the ethanol conversion decreasing from 90 to 40% after 800 min of time on stream (TOS). The decrease in ethanol conversion was accompanied by an increase in acetaldehyde formation and a decrease in CO and methane selectivities.

Recently, da Silva et al. [21] studied the influence of cobalt particle size on the performance of carbon nanofibers (CNF) supported catalysts for SR of ethanol. The use of CNF, generally considered to be an inert support material, allowed to eliminate the interference of other factors on cobalt catalyst activity. It was shown that TOF increased with decreasing Co particle size, which was attributed to a higher density of edge and corner surface sites with decreasing size. Regarding catalyst stability, a decrease in deactivation rate was observed with decreasing cobalt size, due to a significantly lower amount of carbon deposition on the smallest (<3 nm) Co particles than on larger ones, as confirmed by TEM measurements. The reduced amount of carbon deposition was ascribed to a lower fraction of terrace atoms, proposed to be responsible for excessive carbon deposition on catalysts with large (>10 nm) Co particles.

Despite the extensive amount of literature on SR of ethanol, there are only a limited number of studies involving the oxidative steam reforming (OSR) of ethanol over cobalt-based catalysts [1,22]. OSR, also known as autothermal reforming, combines the steam reforming and partial oxidation reactions in one reactor; thus, if carefully balanced, OSR precludes the need for an external heat supply. Furthermore, the addition of oxygen to the feed contributes to a decrease in the rate of carbon formation, which is often proposed to be the main cause of catalyst deactivation [23–26]. However, there are no studies in the literature investigating the performance of carbon supported Co catalysts for the OSR of ethanol neither the impact of Co particle size on catalyst stability. The addition of oxygen to the feed could inhibit the deactivation previously observed during the SR of ethanol over Co/CNF catalysts [21].

The aim of this work was to study the cobalt particle size effects on the catalyst stability during the ethanol oxidative steam reforming reaction by using an inert CNF support material.

2. Experimental

2.1. Catalyst preparation

The carbon nanofiber support material (SA = 200 $m^2\,g^{-1}$, PV = 0.65 $mL\,g^{-1}$) was obtained from synthesis gas using a 5 wt% Ni/SiO_2 growth catalyst. This material was purified in subsequent reflux treatments of 1 M KOH and concentrated HNO_3. In the latter step, oxygen-containing groups required to achieve high metal dispersions were introduced [27]. The cobalt catalysts were obtained using incipient wetness impregnation of cobalt acetate tetrahydrate or cobalt nitrate hexahydrate solutions in either water or ethanol, aiming for various Co loadings as described earlier [28]. After impregnation, the samples were dried at 120 °C. Reduction was conducted at 350 °C for 2 h in a flow of 30 vol% H_2 in N_2, followed by a passivation treatment at room temperature using diluted (0.1%) oxygen flow. In this way, Co/CNF catalysts were obtained with cobalt sizes ranging from 2.6 to 16 nm. The cobalt particle sizes were determined using H_2 chemisorption or X-ray photoelectron spectroscopy (XPS).

2.2. Hydrogen chemisortpion

Co particle size was measured from H_2 chemisorption uptakes using a Micromeritics ASAP 2010C. Before each measurement, the sample was dried in vacuum at 120 °C overnight. Then, the samples were reduced using H_2 by increasing the temperature at 5 K/min to 623 K, and holding at this temperature for 2 h. Following reduction, the samples were evacuated at 623 K for 30 min. The H_2 adsorption isotherms were measured at 423 K. Total hydrogen uptake was determined by extrapolation of the linear part of the isotherm to zero pressure. Particle size estimations were based on hemispherical geometry, assuming that the adsorption stoichiometry H/Co_s is equal to 1:1, and considering the formula $d = 81.6W/X$, with d being the cobalt particle diameter (nm), W is the weight percentage of cobalt, and X is the total H_2 uptake in micromoles per gram of catalyst [29].

2.3. XPS

XPS measurements for passivated samples were carried out using a Vacuum Generators XPS spectrometer with Al Kα radiation. The C 1s binding energy (BE) of 284.6 eV was used to correct for charging effects. The BE values reported here are accurate to ±0.2 eV. The surface atomic ratios were calculated from photoelectron peak areas after correcting for photoionization cross section and the mean free path of photoelectron. The intensity ratio between Co $2p_{3/2}$ and C 1s peaks (I_{Co}/I_C) was used to calculate Co particle size taking into account the procedure described by Kuipers et al. [30].

2.4. Transmission electron microscopy (TEM)

TEM analysis was used to study the Co particle sizes of the fresh and spent catalysts. Catalysts were first suspended in ethanol, and then transferred to a carbon support film on a copper TEM grid. The TEM measurements were conducted with a Tecnai 20 FEG microscope operating at 200 kV.

2.5. Reaction conditions

OSR was performed in a fixed-bed reactor at atmospheric pressure. Prior to reaction, catalysts were reduced at 623 K for 1 h and then purged with N_2 at the same temperature for 30 min. All reactions were carried out at 773 K. OSR was performed employing a H_2O/ethanol molar ratio of 3.0 and an O_2/ethanol molar ratio of 0.5. The reactant mixtures were obtained by flowing 5.6% O_2/N_2 (30 mL/min) and N_2 (30 mL/min) through two saturators containing ethanol and water, respectively, which were maintained at the temperature required to obtain the desired H_2O/ethanol and O_2/ethanol molar ratios.

In order to observe the catalyst deactivation within a short timeframe, a small amount of catalyst was used (20 mg). The samples were diluted with inert SiC. The reaction products were analyzed by gas chromatography (Micro GC Agilent 3000 A) containing three channels for three thermal conductivity detectors (TCD) and three columns: a molecular sieve, a Plot Q, and an OV-1 column. The ethanol conversion and selectivity to products were determined from:

$$X_{\text{ethanol}} = \frac{(n_{\text{ethanol}})_{\text{fed}} - (n_{\text{ethanol}})_{\text{exit}}}{(n_{\text{ethanol}})_{\text{fed}}} \times 100 \quad (1)$$

$$S_x = \frac{(n_x)\ \text{produced}}{(n_{\text{total}})\ \text{produced}} \times 100 \quad (2)$$

where $(n_x)_{\text{produced}}$ = moles of x produced (x = hydrogen, CO, CO_2, methane, acetaldehyde or ethene) and $(n_{\text{total}})_{\text{produced}}$ = moles of H_2 + moles of CO + moles of CO_2 + moles of methane + moles of acetaldehyde + moles of ethene (the moles of water produced are not included).

Table 1
Cobalt on carbon nanofiber catalysts with their preparation details, loadings and particle sizes.

ID	Solvent	Precursor	Co loading (wt%)	H_2-chemisorption (nm)	TEM analysis (nm)
Co16	Water	Cobalt nitrate	22	16	16
Co10	Water	Cobalt nitrate	9.7	9.9	9.7
Co5	Ethanol	Cobalt nitrate	3.5	4.8	–
Co3	Water	Cobalt acetate	0.9	2.9[a]	2.8

[a] Co particle size determined by XPS.

3. Results and discussion

3.1. Catalyst characterization

The Co/CNF catalysts with their properties and preparation routes are summarized in Table 1. The cobalt particle sizes calculated by H_2 chemisorption and XPS varied from 2.6 to 16 nm as cobalt loading increased from 1.0 to 22 wt%.

3.2. OSR of ethanol

Fig. 1 shows the ethanol conversion and product distributions as a function of TOS during OSR over Co3 and Co16 catalysts. The Co5 and Co10 catalysts (data not shown) exhibited approximately the same result as observed for the Co16 catalyst.

The catalyst containing the smallest Co particle sizes (2.9 nm) exhibited a slow deactivation, with the ethanol conversion continuously decreasing during 25 h TOS from 97 to 90%. Hydrogen selectivity slightly decreased, following the same trend as ethanol conversion, whereas acetaldehyde selectivity increased. The selectivity to CO_2 and CO remained approximately constant at 35 and 14%, respectively.

For the Co5, Co10 and Co16 catalysts, ethanol was completely consumed and its conversion remained approximately constant during 25 h of TOS. Hydrogen (55%) and CO_2 (35%) were the main

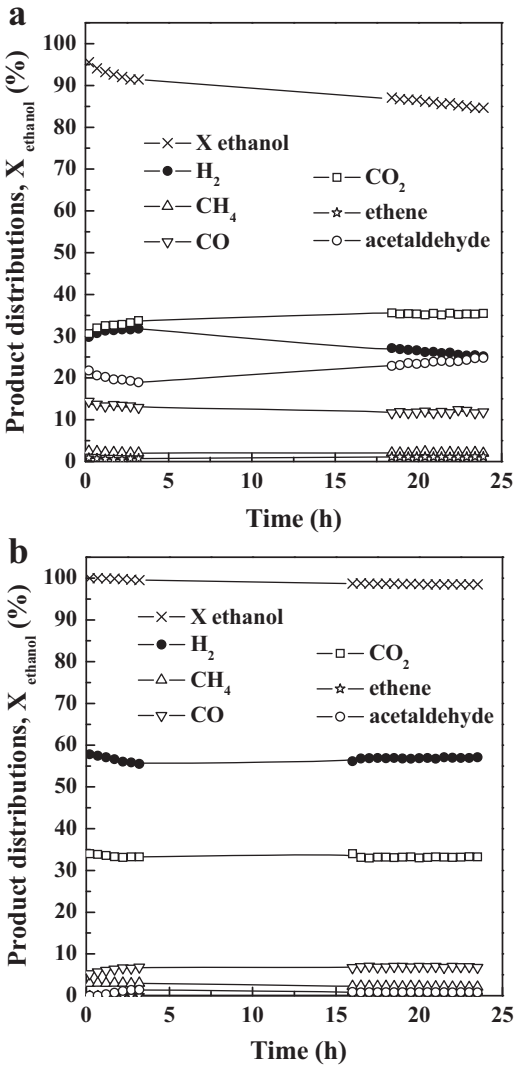

Fig. 1. Ethanol conversion ($X_{ethanol}$) and product distributions versus time on stream obtained on OSR under H_2O/ethanol molar ratio = 3.0 and O_2/ethanol molar ratio = 0.5 over (a) Co3; (b) Co16 ($T_{reaction}$ = 773 K and residence time = 0.02 g s/mL).

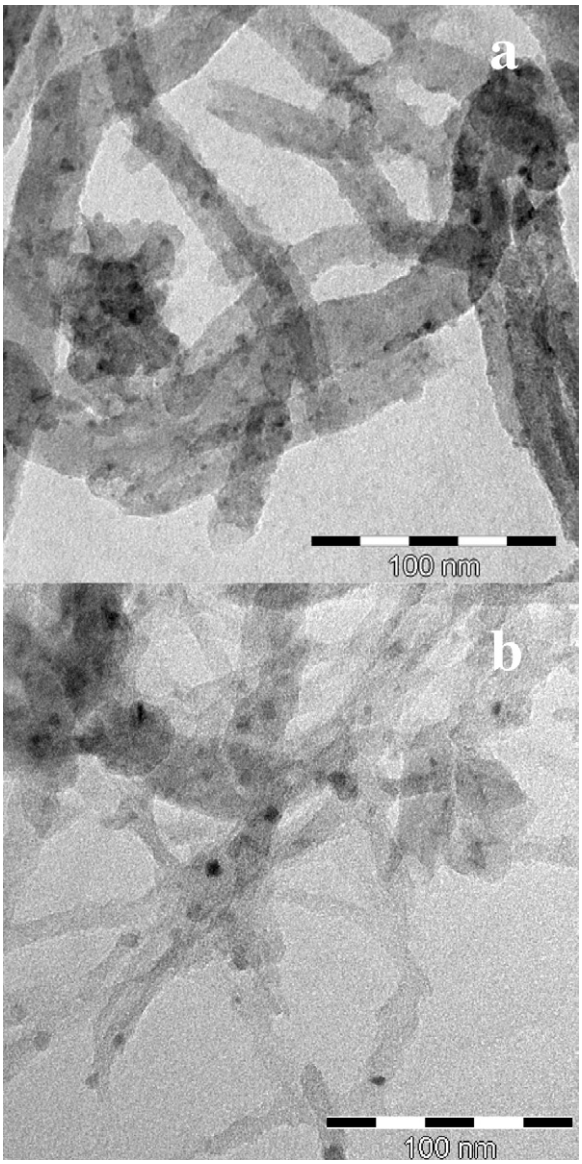

Fig. 2. TEM images of the fresh (a) and spent (b) Co3 catalyst.

products formed while only small amounts of acetaldehyde (3%) were detected after 25 h of TOS.

The addition of oxygen to the feed significantly increased ethanol conversion in comparison to the ethanol conversion obtained in the SR reaction using the same Co/CNF catalysts [21]. Furthermore, hydrogen selectivity decreased whereas CO_2 formation increased when oxygen was present in the feed. Cai et al. [26] compared the performance of Ir/CeO_2 catalyst for SR and OSR. They observed that the reaction rate of OSR was higher than that of SR, indicating that oxygen addition promoted the surface reaction of ethanol. They proposed that the lattice oxygen atoms of ceria participate in activating the ethanol molecule. Kugai et al. [23] also studied the performance of $Ni–Rh/CeO_2$ catalyst for SR and OSR. The addition of oxygen to the feed also increased ethanol conversion, attributed to the higher C–C bond cleavage capacity by oxygen. The ethanol conversion rates observed for OSR over $Pt/CeZrO_2$ were also higher than those detected for the case of SR reaction. [31]. DRIFTS analysis revealed that the presence of oxygen promoted the ethanol dehydrogenation reaction to acetaldehyde as well as the oxidation of ethoxy species to acetate, followed by the decomposition to CO_2 via carbonate species. These reaction pathways may explain the higher ethanol conversion observed for Co/CNF catalysts in the OSR reaction as compared to the SR of ethanol.

Compared to the SR of ethanol [21], the presence of oxygen in the feed also significantly improved Co/CNF catalyst stability. The catalysts containing larger Co particle sizes (>4 nm) showed a significant decrease in conversion with TOS during SR of ethanol whereas they were quite stable during OSR. Next, the reasons for catalyst deactivation will be discussed in more detail.

3.3. Catalyst deactivation

The stability of Co-based catalysts is the most important issue during ethanol conversion reactions to produce hydrogen. Three main causes for catalyst deactivation are reported in the literature: (i) carbon deposition [1,32,33]; (ii) Co sintering [10]; and (iii) oxidation of Co metallic particles [22].

In our work, a TEM study was performed to determine the main drivers of Co/CNF catalyst deactivation by measuring the extent of Co particle sintering as well as characterizing the nature of the carbonaceous species formed during OSR. TEM images of Co3 and Co16 catalysts before and after OSR of ethanol at 773 K are shown in Figs. 2 and 3.

TEM images of the reduced and passivated samples reveal the presence of cobalt particles decorating rather long fibers (Figs. 2a and 3a). Representative TEM images of the spent Co3 catalyst (Fig. 2b) did not show significant formation of amorphous or filamentous carbon during OSR. On the other hand, the TEM images of the spent catalyst containing large Co particle sizes show the presence of two types of carbon deposits: (i) an amorphous carbon layer covering the catalyst surface (Fig. 3b) and (ii) carbon filaments containing the Co particle at the end (Fig. 3c). This is not

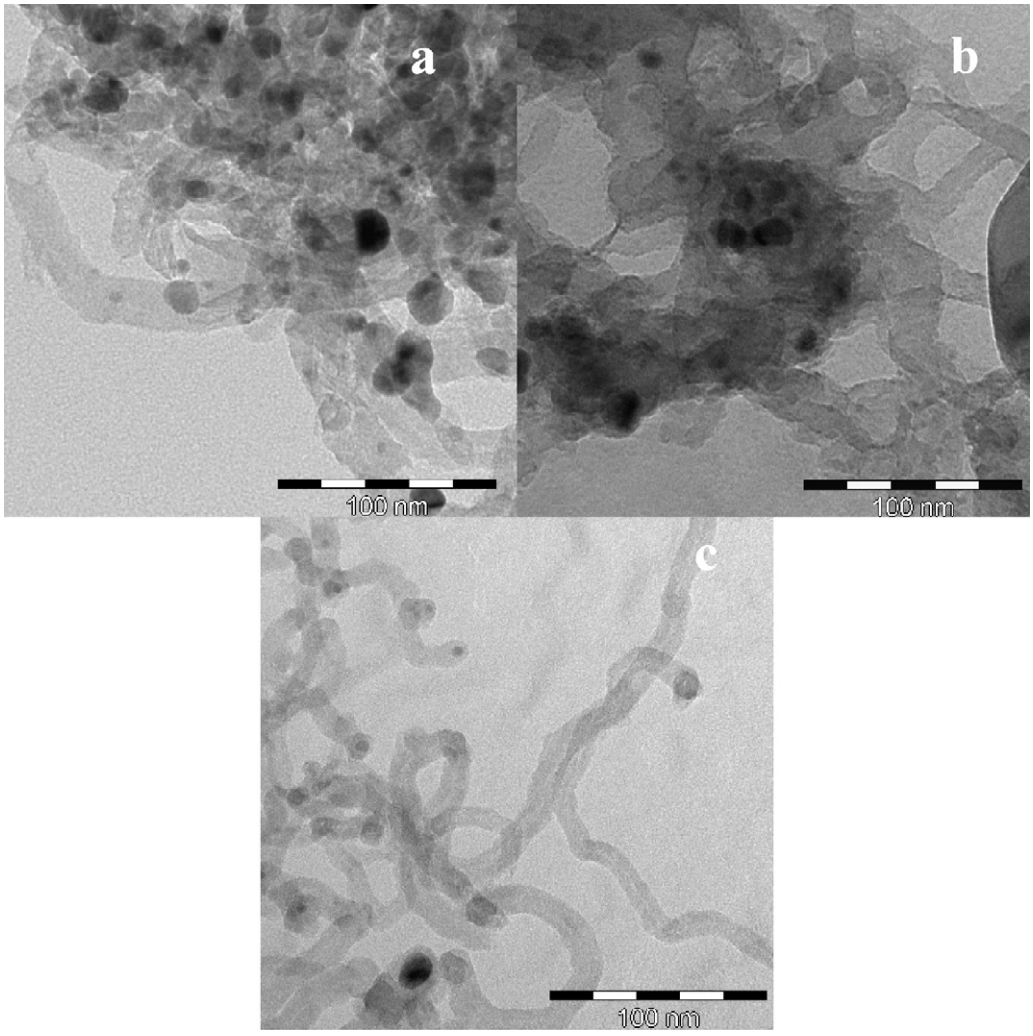

Fig. 3. TEM images of the fresh (a) and spent (b and c) Co16 catalyst.

the nickel growth catalyst used to make the parent fibers, since it was removed prior to the preparation of the Co/CNF catalysts. In comparison to the Co16 spent catalyst after SR [21], lower amounts of amorphous carbon seems to be present after OSR.

The cobalt particle sizes of the fresh and spent catalysts were determined from the TEM images. For the Co3 catalyst, the cobalt particle size changed from 2.9 nm for the fresh catalyst to 4.1 nm for the spent catalyst, indicating a minor sintering during OSR reaction. For the Co16 catalyst, only a slight increase in size from 16 to 18 nm was observed, which means that no significant sintering was observed on this catalyst. The Co16 spent catalyst also contained a significant amount of smaller (5–12 nm) Co particles entrapped in a fibrous material.

To investigate the possibility of cobalt oxidation during the reaction, the OSR over Co3 and Co16 was carried out over the unreduced catalyst (Fig. 4). The unreduced samples exhibit a higher selectivity to acetaldehyde and a lower selectivity to hydrogen than the reduced ones after 24 h of TOS. For instance, acetaldehyde was not detected during the OSR over reduced Co16 catalyst whereas a significant formation of acetaldehyde is observed for the unreduced Co16 sample (Fig. 4b). A comparison between the product distribution for OSR over the reduced (Fig. 1a) and unreduced (Fig. 4a) Co3 catalyst indicates that the oxidation of Co particles occurs and it is likely the main reason for the deactivation of the Co3 catalyst. This result also suggests that small Co particles were more easily oxidized than the larger ones during OSR.

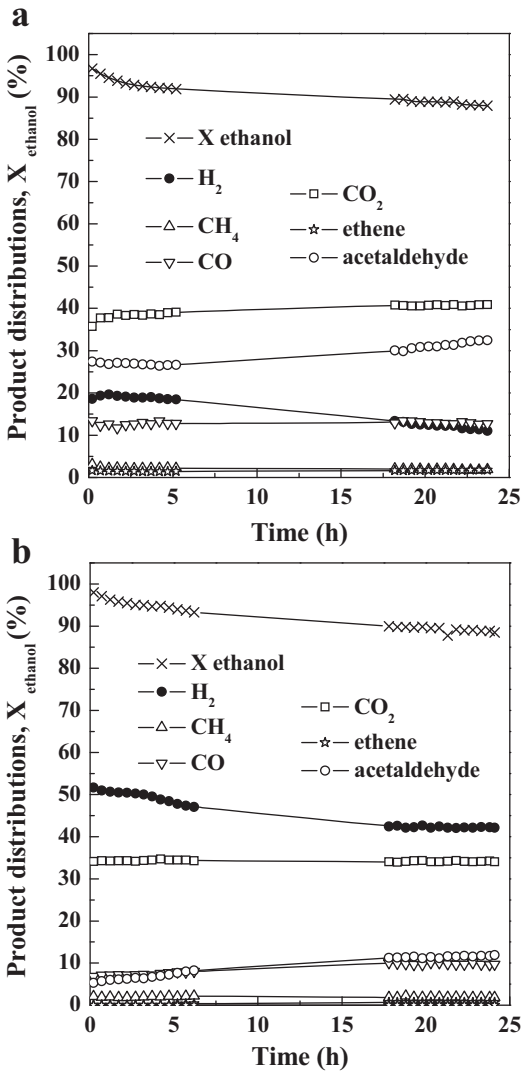

Fig. 4. Ethanol conversion ($X_{ethanol}$) and product distributions versus time on stream over unreduced (a) Co3 and (b) Co16 catalysts obtained during OSR (H_2O/ethanol molar ratio = 3.0 and O_2/ethanol molar ratio = 0.5; $T_{reaction}$ = 773 K and residence time = 0.02 g s/mL).

3.4. General discussion

Recently, we demonstrated that Co/CNF catalysts containing large (>4 nm) Co particles underwent severe deactivation, mainly caused by amorphous carbon deposition. This was ascribed to a higher fraction of terrace sites on large Co particles [21].

According to the literature [23–26], the addition of oxygen to the feed promotes the removal of carbon species formed during the reaction. Therefore, the OSR of ethanol could inhibit the deactivation observed on Co/CNF catalysts with large particle sizes.

The catalytic results revealed that the presence of oxygen in the reactant mixture improved catalyst stability. Nevertheless, the TEM images of the spent catalyst showed the formation of filamentous carbon with the Co particle located at the end, indicating that carbon deposition still takes place.

Studies concerning carbon formation over Ni and Co-based catalysts during SR of ethanol are relatively scarce and the mechanism of coke formation is not well established as for example in the case of steam reforming of methane. We recently studied the mechanism of catalyst deactivation for SR and OSR of ethanol over $Pt/CeZrO_2$ and Co/CeO_2 catalysts [1,14,31]. According to the proposed reaction mechanism for SR, ethanol adsorbs dissociatively to form ethoxy species on the surface. The ethoxy species is dehydrogenated to acetaldehyde and acetyl species, which may be further oxidized to acetate species. The decomposition of dehydrogenated species (e.g., acetaldehyde, acetyl) and acetate species produce hydrogen, CO, and CH_x species, which may in turn result in carbon formation depending on the rate of hydrogen recombination. Therefore, the catalyst should deactivate when the rate of this reaction pathway is higher than the rate of desorption of CH_x species as CH_4. The CH_x species formed may block the metal surface resulting in catalyst deactivation. The CH_x species may be further dehydrogenated to H and C. In the case of Co based catalysts, this highly reactive carbon species formed will either (a) react with O_2 (or H_2O) to produce CO_X species; (b) encapsulate the Co particle; or (c) diffuse through the Co crystallite followed by the nucleation and growth of carbon filaments (e.g., whiskers). This is similar to the mechanism proposed for growth of filamentous carbon by decomposition of ethanol on Ni foam [34]. Although the Co/CeO_2 catalyst was quite stable during OSR of ethanol at 773 K, TEM images of spent catalyst revealed the presence of several carbon nanotubular structures or filaments [1]. Actually, the addition of oxygen to the feed helped to maintain the surface of the metal clean, keeping it active for a longer period of time. Therefore, the metal can remain active despite having a considerable amount of carbon deposited behind the particles, since the top surface will remain exposed to reactants and gas-phase intermediates. According to Trimm [35], this is a special case where coke formation does not result in catalyst deactivation.

In the case of OSR, the oxidation of metallic particles by the oxygen from the feed is another potential cause for catalyst deactivation. The OSR of ethanol has been less studied than SR in the literature [22–26,36–39] and only two papers involve Co-based catalysts [1,22].

Pereira et al. [22] reported that Co/SiO_2, $Co–Rh/SiO_2$ and $Co–Ru/SiO_2$ catalysts deactivate when OSR of ethanol is carried out between temperatures of 623 and 673 K. The decrease in ethanol conversion was accompanied by a decrease in hydrogen selectivity and an increase in acetaldehyde selectivity. Catalyst deactivation was attributed to the oxidation of the surface of Co particles by oxygen from the feed and the cobalt oxide formed favored dehy-

drogenation of ethanol to acetaldehyde. On the bimetallic catalysts, the addition of a noble metal (e.g., Rh, Ru) stabilized the Co in the reduced state (active phase for the SR of ethanol), preventing the oxidation of cobalt particles. The deactivation of $NiRh/CeO_2$ catalyst during OSR at 623 K was also attributed to the passivation of the catalyst surface by oxygen from the feed [36]. Laosiripojana et al. [37] demonstrated that there is an optimal O_2/ethanol ratio above which Ni oxidation to NiO takes place, resulting in a decrease of reforming activity.

For the Co/CNF catalyst with small Co particle size, the similarity between the product distribution of the tests carried out over unreduced and reduced catalysts indicates that SR of ethanol reaction is not favored during OSR over the small Co particles. This might be due to partial surface oxidation, which could be responsible for changes in selectivities and also catalyst deactivation. De la Pena O'Shea studied the SR of ethanol over Co_3O_4 by in situ X-ray diffraction coupled with gas chromatography [15]. They demonstrated that the dehydrogenation of ethanol to acetaldehyde is the main reaction in presence of cobalt oxide, which agrees very well with our results.

3.5. Conclusions

Cobalt on carbon nanofiber catalysts with different Co particle sizes (2.6–16 nm) were tested in the OSR of ethanol reaction to produce hydrogen. High ethanol conversions (>85%) were obtained, however at the expense of the H_2-selectivity in comparison to SR. Moreover, a lower amount of carbon was deposited as compared to SR of ethanol reaction. However, the catalysts with the lowest Co particle size deactivated most likely due to oxidation of surface atoms by oxygen from the feed whereas the catalysts with large Co particle size (>4 nm) remained quite stable.

Acknowledgements

The authors acknowledge CTENERG/FINEP-01.04.0525.00 and Shell Global Solutions for financial support. C. van der Spek is thanked for TEM analyses and Dr. Bezemer for some Co/CNF catalysts.

References

[1] S.M. de Lima, A.M. da Silva, L.O.O. da Costa, U.M. Graham, G. Jacobs, B.H. Davis, L.V. Mattos, F.B. Noronha, J. Catal. 268 (2009) 268.
[2] J. Llorca, N. Homs, P.R. de la Piscina, J. Catal. 227 (2004) 556.
[3] J. Llorca, P.R. de la Piscina, J. Sales, N. Homs, Chem. Commun. (2001) 641.
[4] J. Llorca, N. Homs, J. Sales, P.R. de la Piscina, J. Catal. 209 (2002) 306.
[5] J.C. Vargas, S. Libs, A.C. Roger, A. Kiennemann, Catal. Today 107 (2005) 417.
[6] H. Song, L. Zhang, R.B. Watson, D. Braden, U.S. Ozkan, Catal. Today 129 (2007) 346.
[7] H. Song, B. Tan, U.S. Ozkan, Catal. Lett. 132 (2009) 422.
[8] J.M. Guil, N. Homs, J. Llorca, P.R. de la Piscina, J. Phys. Chem. B 109 (2005) 10813.
[9] B. Zhang, X. Tang, Y. Li, W. Cai, Y. Xu, W. Shen, Catal Commun. 7 (2006) 367.
[10] H. Song, U.S. Ozkan, J. Catal. 261 (2009) 66.
[11] R.U. Ribeiro, J.W.C. Liberatori, H. Winnishofer, J.M.C. Bueno, D. Zanchet, Appl. Catal., B 91 (2009) 670.
[12] A.N. Fatsikostas, X.E. Verykios, J. Catal. 225 (2004) 439.
[13] S.M. de Lima, R.C. Colman, G. Jacobs, B.H. Davis, K.R. Souza, A.F.F. de Lima, L.G. Appel, L.V. Mattos, F.B. Noronha, Catal. Today 146 (2009) 110.
[14] S.M. de Lima, A.M. Silva, U.M. Graham, G. Jacobs, B.H. Davis, L.V. Mattos, F.B. Noronha, Appl. Catal., A 352 (2009) 95.
[15] V.A. de La Pena O'Shea, N. Homs, E.B. Pereira, R. Nafria, P.R. de la Piscina, Catal. Today 126 (2007) 148.
[16] E. van Steen, M. Claeys, M.E. Dry, J. van de Loosdrecht, E.L. Viljoen, J.L. Visagie, J. Phys. Chem. B 109 (2005) 3575.
[17] V.V. Galvita, G.L. Semin, V.D. Belyaev, V.A. Semikolenov, P. Tsiakaras, V.A. Sobyanin, Appl. Catal., A: Gen. 220 (2001) 123.
[18] V.V. Galvita, V.D. Belyaev, V.A. Semikolenov, P. Tsiakaras, A. Frumin, V.A. Sobyanin, React. Kinet. Catal. Lett. 76 (2002) 343.
[19] F. Haga, T. Nakajima, H. Miya, S. Mishima, Catal. Lett. 48 (1997) 223.
[20] R. Barthos, A. Szechenyi, F. Solymosi, Catal. Lett. 120 (2008) 161.
[21] A.L.M. da Silva, L.V. Mattos, J. von Breen, J.H. Bitter, K.P. de Jong, F.B. Noronha, Book of Abstracts of NGCS 9, 2010 (Lyon, France, paper KN06).
[22] E.B. Pereira, N. Homs, S. Marti, J.L.G. Fierro, P.R. de la Piscina, J. Catal. 257 (2008) 206.
[23] J. Kugai, S. Velu, C. Song, Catal. Lett. 101 (2005) 255.
[24] V. Fierro, O. Akidim, C. Mirodatos, Green Chem. 5 (2003) 20.
[25] R.M. Navarro, M.C. Alvarez-Galvan, M. Cruz Sanchez-Sanchez, F. Rosa, J.L.G. Fierro, Appl. Catal., B: Environ. 55 (2005) 229.
[26] W. Cai, F. Wanga, E. Zhan, A.C. Van Veen, C. Mirodatos, W. Shen, J. Catal. 257 (2008) 96.
[27] M.K. Van der Lee, A. Van Jos Dillen, J.H. Bitter, K.P. De Jong, J. Am. Chem. Soc. 127 (2005) 13573.
[28] G.L. Bezemer, J.H. Bitter, H.P.C.E. Kuipers, H. Oosterbeek, J.E. Holewijn, X. Xu, F. Kapteijn, A.J. van Dillen, K.P. de Jong, J. Am. Chem. Soc. 128 (2006) 3956.
[29] R.C. Reuel, C.H. Bartholomew, J. Catal. 85 (1984) 63.
[30] H.P.C.E. Kuipers, H.C.E. van Leuven, W.M. Visser, Surf. Interface Anal. 8 (1986) 235.
[31] S.M. de Lima, I.O. da Cruz, G. Jacobs, B.H. Davis, L.V. Mattos, F.B. Noronha, J. Catal. 257 (2008) 96.
[32] A.E. Galetti, M.F. Gomez, L.A. Arrua, A.J. Marchi, M.C. Abello, Catal. Commun. 9 (2008) 1201.
[33] H. Wang, Y. Liu, L. Wang, Y.N. Qin, Chem. Eng. J. 145 (2008) 25.
[34] N. Jeong, J. Lee, J. Catal. 260 (2008) 217.
[35] D.L. Trimm, Catal. Today 37 (1997) 233.
[36] J. Kugai, S. Velu, C. Song, M.H. Engelhard, Y. Chin, J. Catal. 238 (2006) 430.
[37] N. Laosiripojana, S. Assabumrungrat, Appl. Catal., A 327 (2007) 180.
[38] P. Biswas, D. Kunzru, Catal. Lett. 118 (2007) 36.
[39] J.L. Bi, Y.Y. Hong, C.C. Lee, C.T. Yeh, C.B. Wang, Catal. Today 129 (2007) 322.